Electronic Supplementary Information

Magnetic field assisted electrocatalytic oxygen evolution reaction of nickel-based materials

Yuanyuan Zhang [a], Ping Guo [a], Siwei Li [a], Jianmin Sun [a], Wei Wang [b], Bo Song [b], Xiaoxuan Yang [c], Xianjie Wang [b], Zaixing Jiang [b], Gang Wu [*c] and Ping Xu [*a]

[a] MIIT Key Laboratory of Critical Materials Technology for New Energy Conversion and Storage, School of Chemistry and Chemical Engineering, [b] School of Physics, Harbin Institute of Technology, Harbin 150001, China.

[c] Department of Chemical and Biological Engineering, University at Buffalo, The State University of New York, Buffalo, New York, 14260, United States

Corresponding Author

*Email: pxu@hit.edu.cn (P.X.); gangwu@buffalo.edu (G.W.)

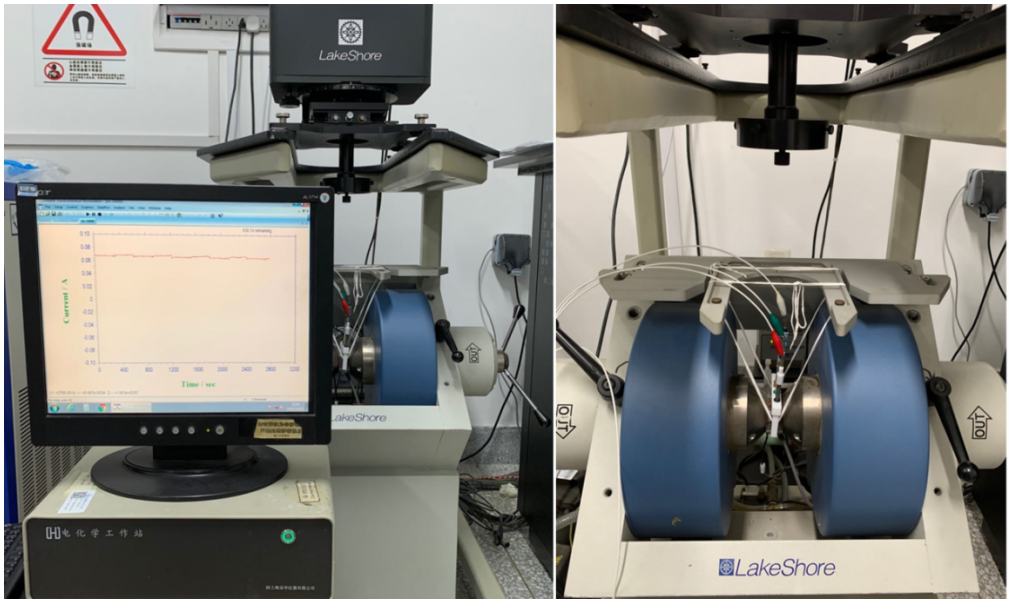

Fig. S1. Physical photographs of our designed three-electrode OER test system coupling a 7400 Series VSM System and an electrochemical workstation.

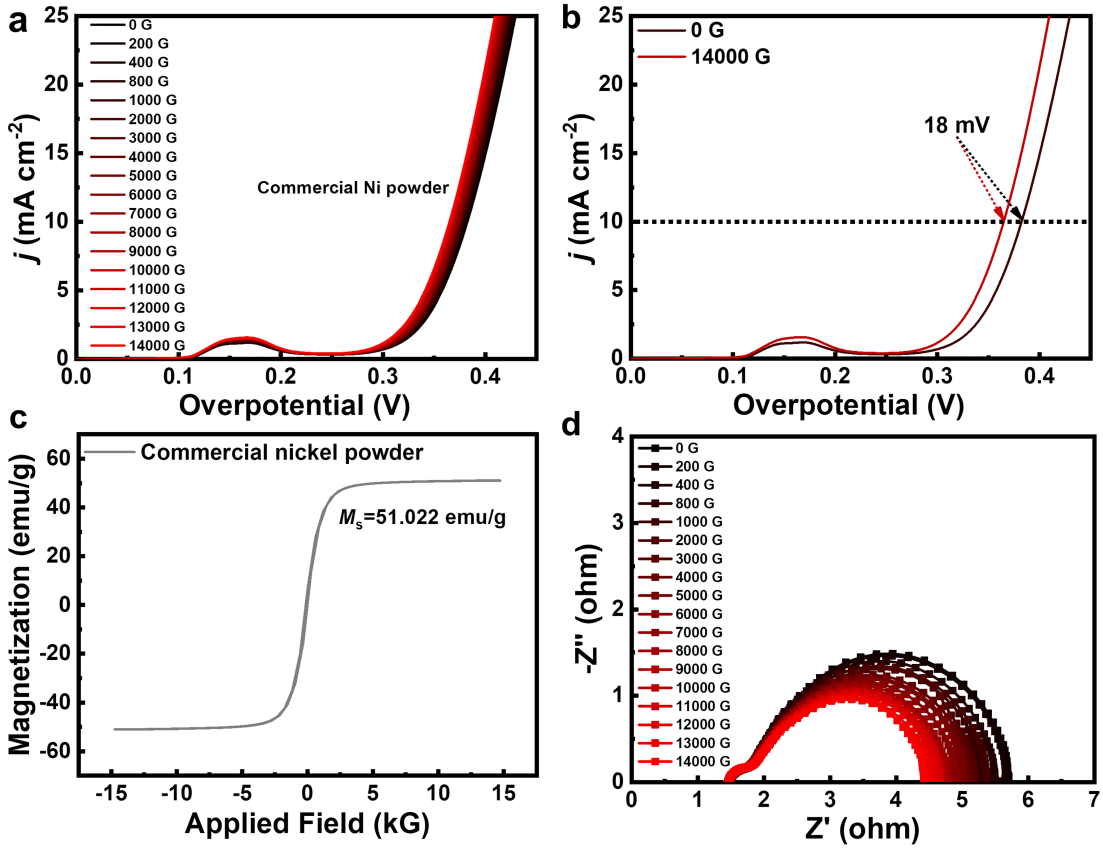

Fig. S2. (a, b) Polarization curves of commercial Ni power supported on carbon cloth electrodes without (OFF, black line), and with an applied magnetic field (ON, red line). (c) hysteresis loop of commercial Ni power. (d) The Nyquist plots of commercial Ni power under magnetic field from 0 to 14000 G.

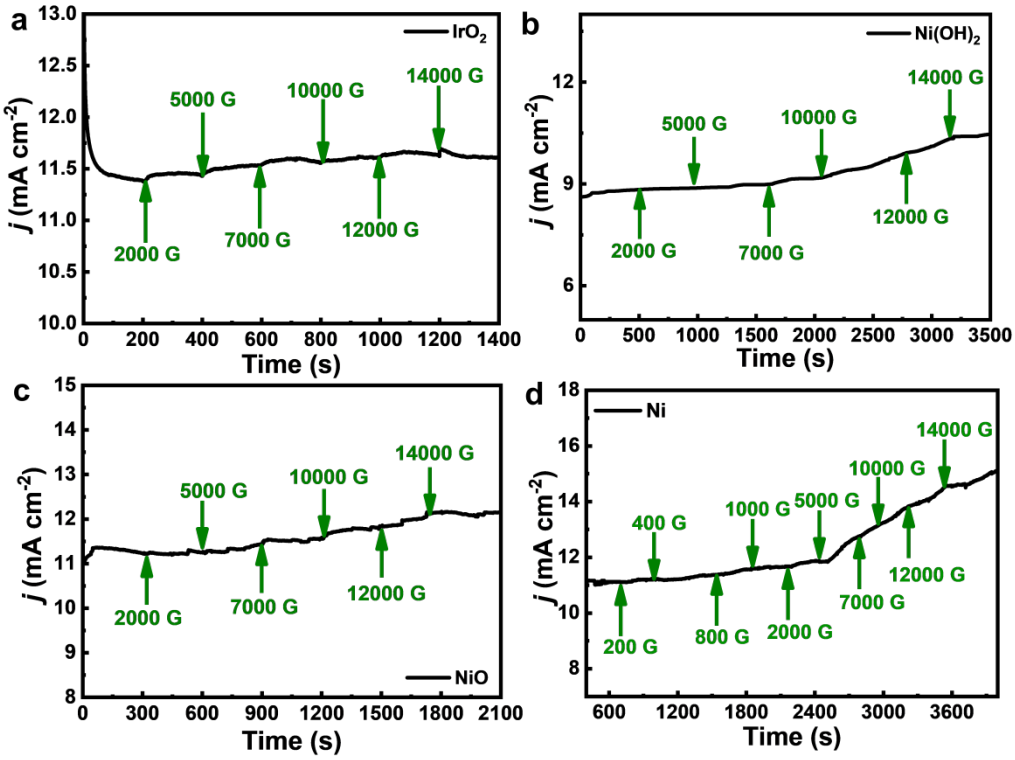

Fig. S3. *I-t* curves of (a) IrO_2, (b) $Ni(OH)_2$, (c) NiO, and (d) Ni continuous application of 2000, 5000, 7000, 10000, 12000, 14000 G.

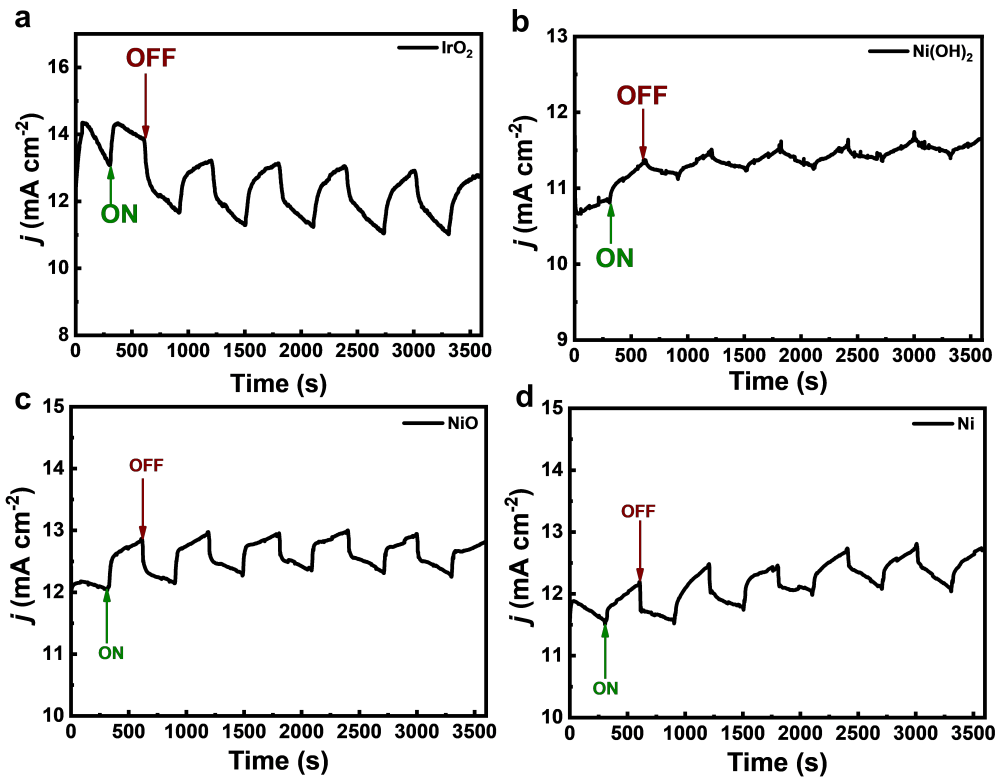

Fig. S4. *I-t* curves of (a) IrO_2, (b) $Ni(OH)_2$, (c) NiO, and (d) Ni under the zero field or magnetic field (14000 G).

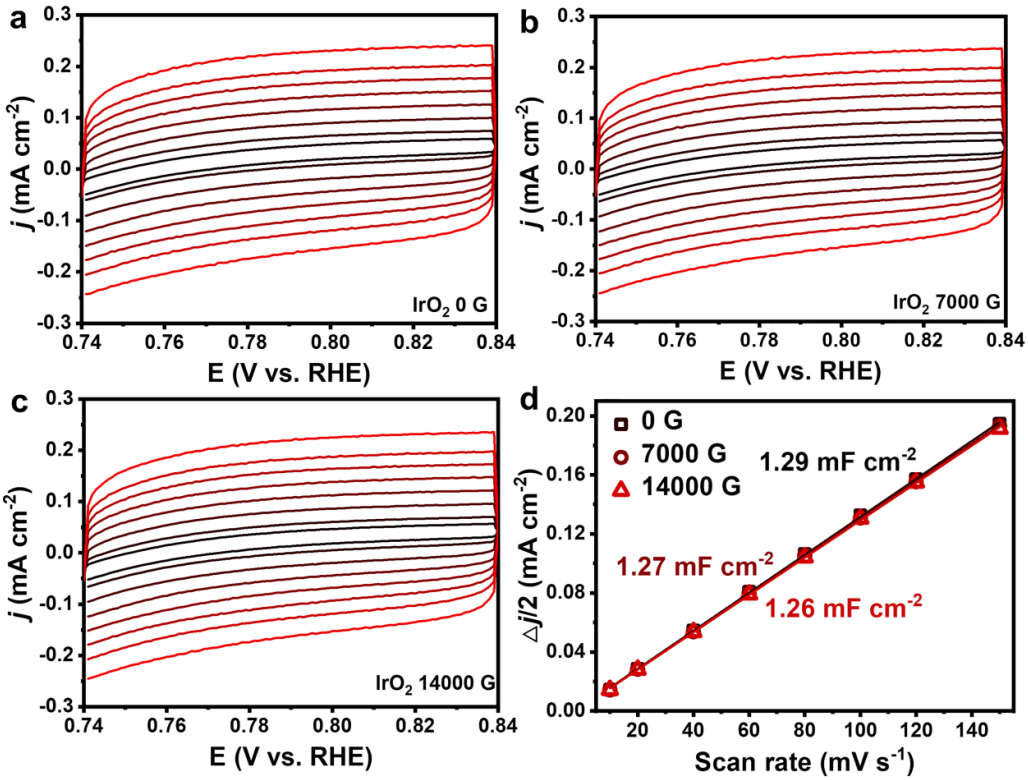

Fig. S5. The CV curves of IrO_2 under a magnetic field of (a) 0 G, (b) 7000 G, and (c) 14000 G. (d) Plots of $\Delta j/2$ vs. scan rates of IrO_2 under different intensities of a magnetic field.

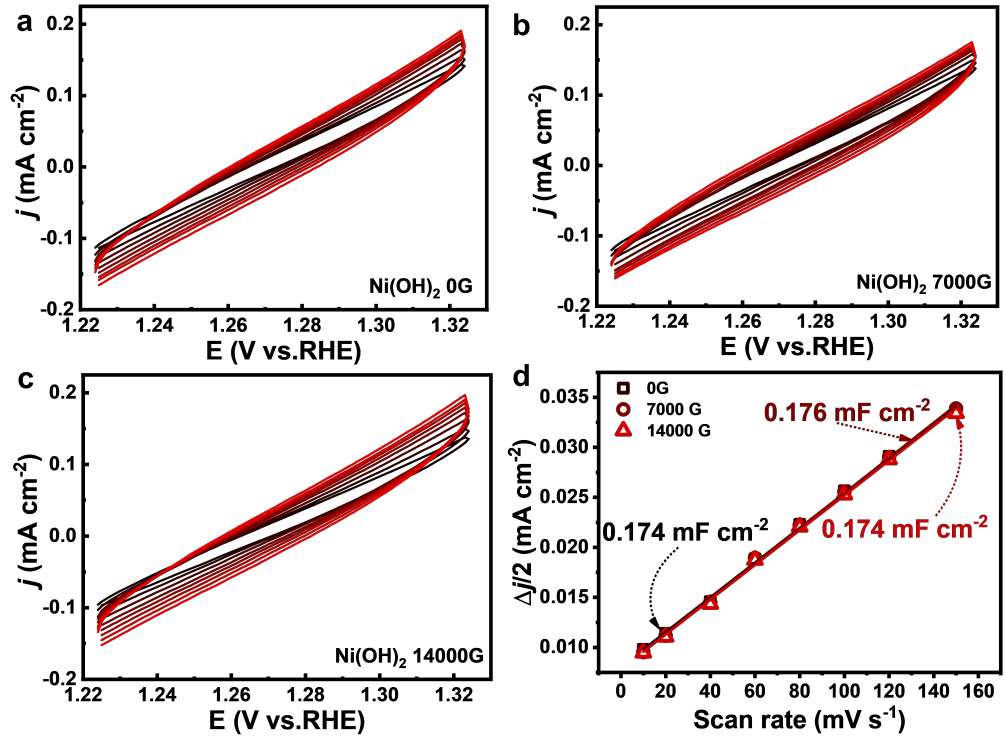

Fig. S6. The CV curves of $Ni(OH)_2$ under a magnetic field of (a) 0 G, (b) 7000 G, and (c) 14000 G. (d) Plots of $\Delta j/2$ vs. scan rates of IrO_2 under different intensities of a magnetic field.

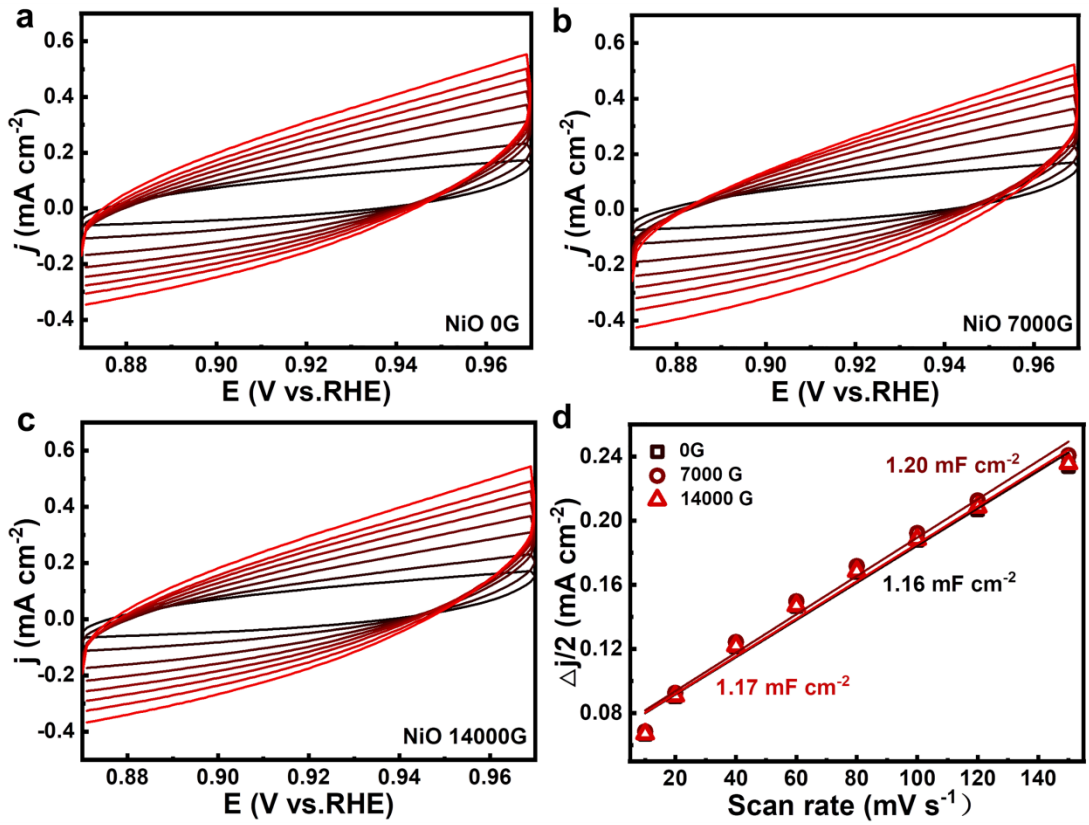

Fig. S7. The CV curves of NiO under a magnetic field of (a) 0 G, (b) 7000 G, and (c) 14000 G. (d) Plots of $\Delta j/2$ vs. scan rates of NiO under the different intensities of a magnetic field.

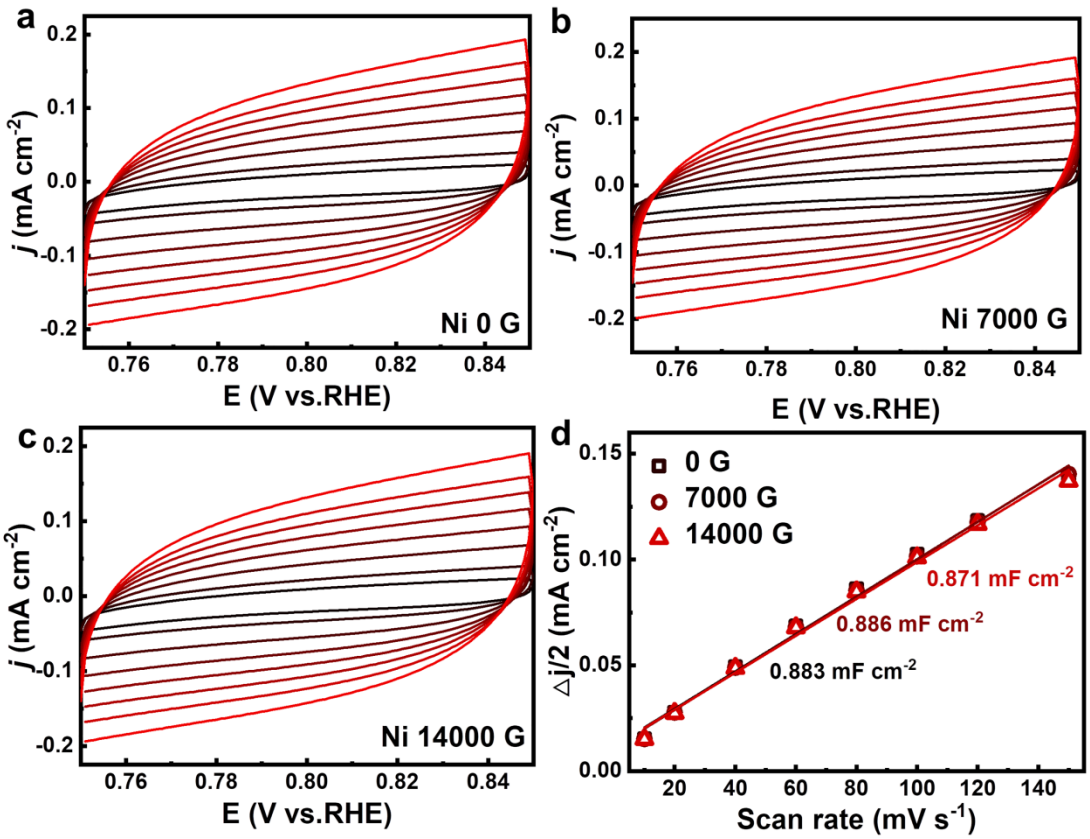

Fig. S8. The CV curves of Ni under a magnetic field of (a) 0 G, (b) 7000 G, and (c) 14000 G. (d) Plots of $\Delta j/2$ vs. scan rates of Ni under the different intensities of a magnetic field.

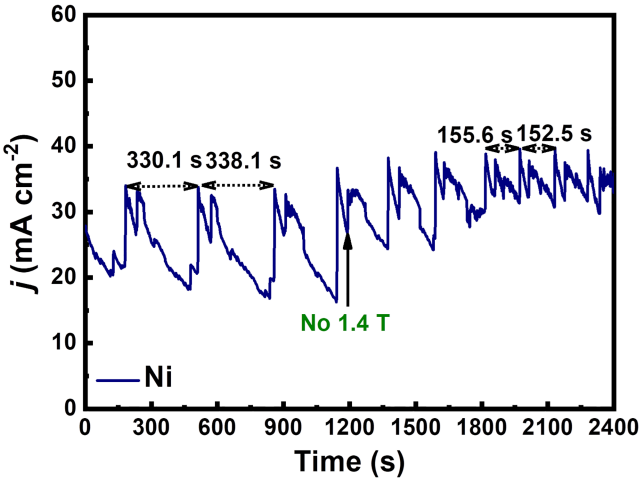

Fig. S9. *I-t* curve of Ni supported on glassy carbon electrode under the zero field or magnetic field (14000 G).

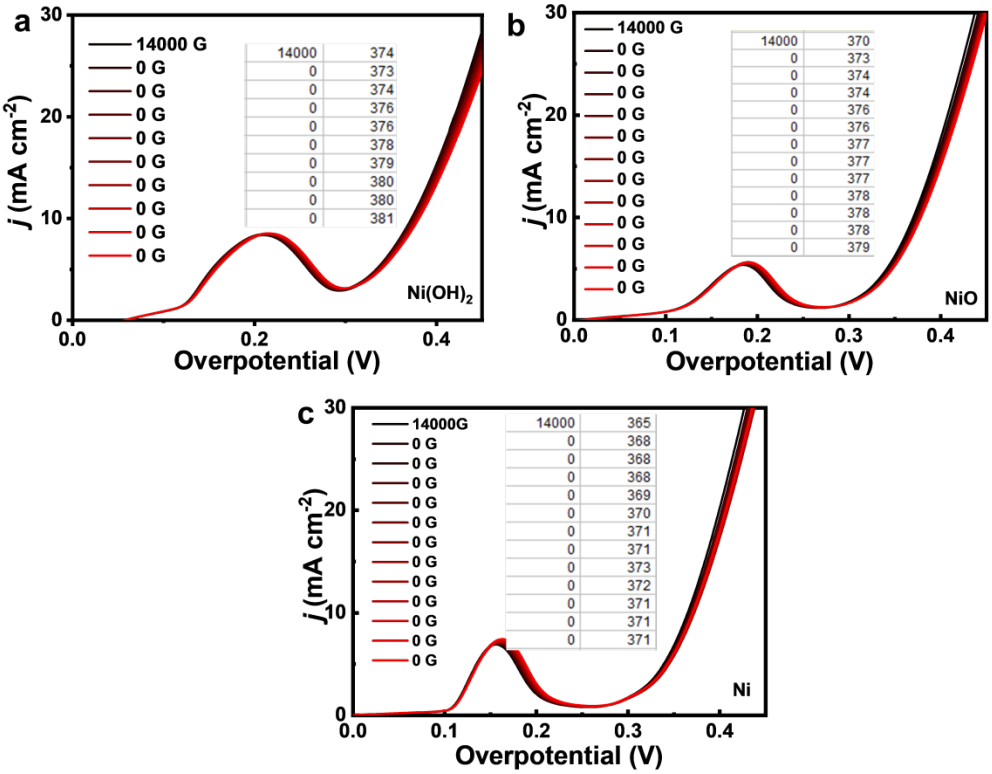

Fig. S10. Polarization curves of various OER catalysts under the action of magnetic field and after removing the magnetic field.

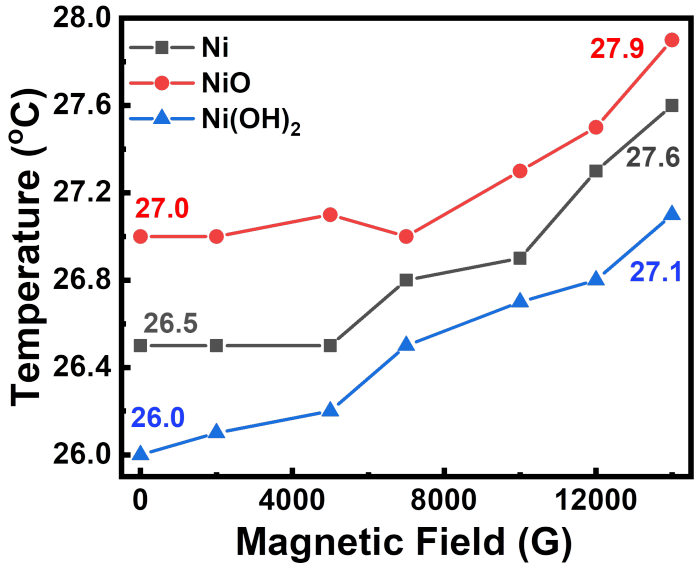

Fig. S11. The temperature changes of the electrolyte solution when $Ni(OH)_2$, NiO, and Ni were applied as the catalysts with different magnetic field intensities during the continuous *I-t* process.

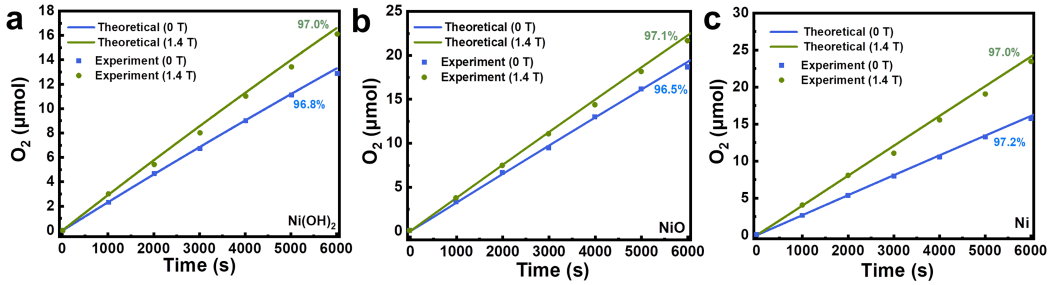

Fig. S12. Determination of Faradaic efficiency. The theoretical and experimental O_2 evolution amount were obtained by electrocatalysis with $Ni(OH)_2$, NiO, and Ni at a anodic current density of 30 mA cm^{-2} for 6000 s under the zero field or magnetic field (14000 G).

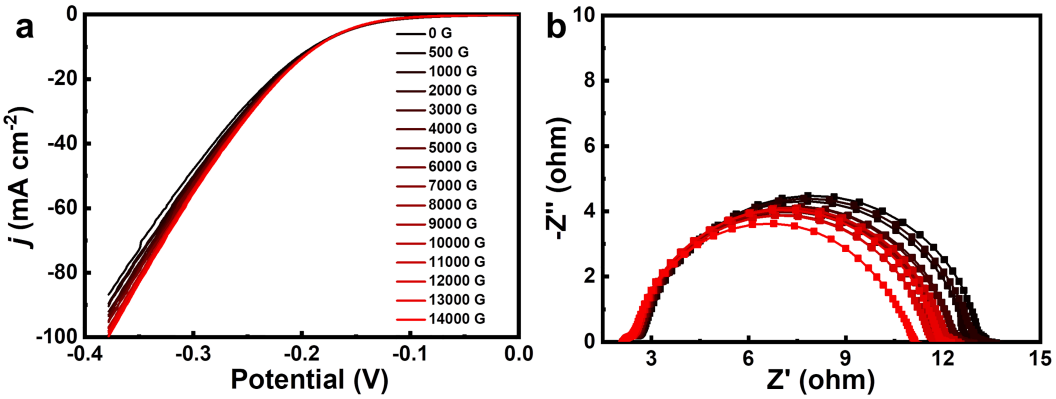

Fig. S13. (a) Polarization curves and (b) Nyquist plots of Ni as HER catalyst under different magnetic fields.

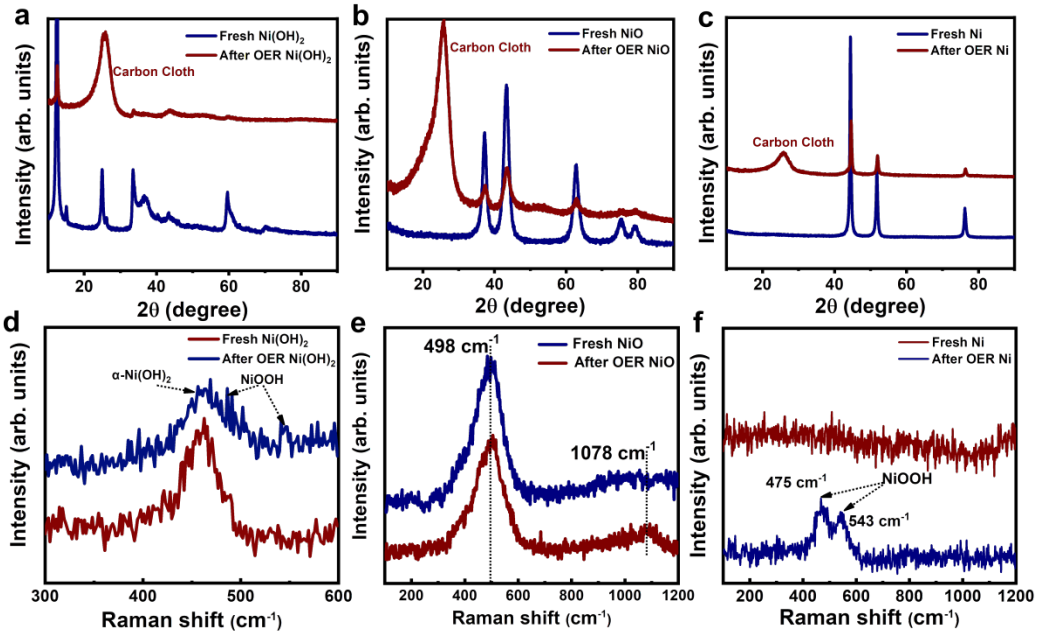

Fig. S14. XRD patterns and Raman spectrometry of (a, d) $Ni(OH)_2$, (b, e) NiO and (c, f) Ni after OER.

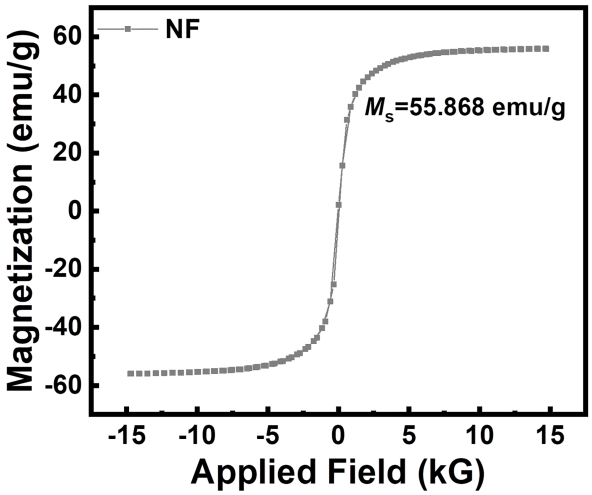

Fig. S15. Hysteresis loop of Ni foam.

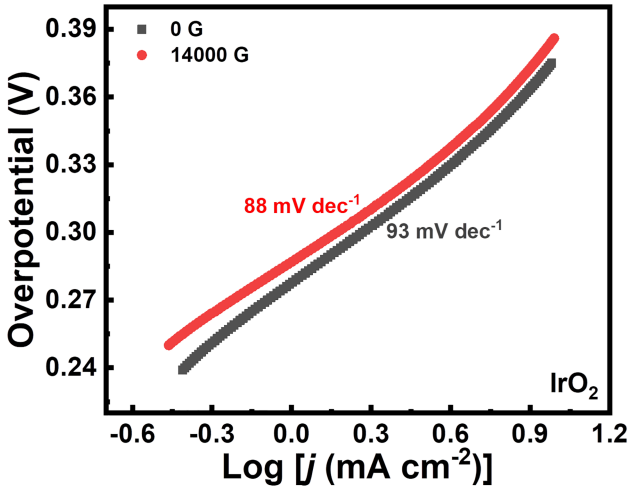

Fig. S16. Tafel slopes of IrO_2 under the zero field or magnetic field (14000 G).

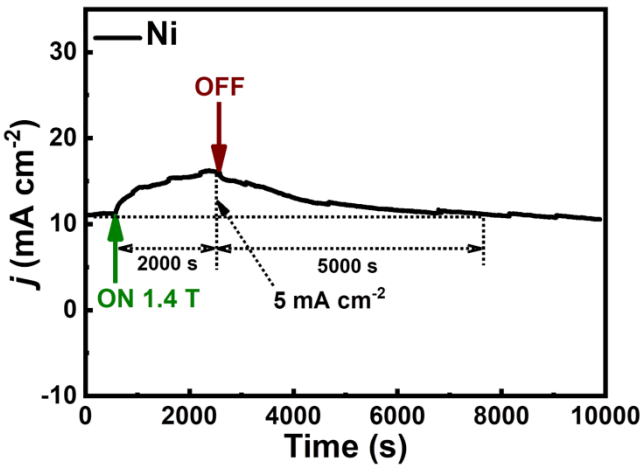

Fig. S17. *I-t* curve of ferromagnetic Ni (coercivity~57.4 Oe) under a magnetic field of 14000 G (2000 s) after the current gets stabilized and then removed the magnetic field.

Table S1. Charge transfer resistance (R_{ct}) of different catalysts without/with magnetic field.

Catalysts	R_{ct}(0 G)	R_{ct}(14000 G)
IrO_2	5.009	4.054
$Ni(OH)_2$	2.412	1.997
NiO	2.437	1.727
Ni	2.765	1.766

Table S2. Charge transfer resistance (R_{ct}) of Ni Foam in different electrolyte concentrations without/with a magnetic field.

Electrolyte	R_{ct}(0 G)	R_{ct}(14000 G)
0.1 M KOH	12.600	3.129
1 M KOH	8.432	3.296
3 M KOH	6.514	4.591

Table S3. Magnetic field enhanced the electrocatalytic performance of different Catalysts.

Catalyst	type of electrocatalytic reaction	electrolyte	magnetic field intensity	Catalytic performance	Ref
NF/Co_3O_4	OER	1 M KOH	55-125 mT	the overpotential decreased 252 mV@20 mA cm^{-2}	1
$NiZnFe_4O_x$	OER	1 M KOH	≤450 mT	current density increases 16 mA cm^{-2} @1.65 V	2
NiCoFe-MOF-74	OER	1 M KOH	0-5.616 mT	the overpotential decreased 124 mV@10 mA cm^{-2}	3
$CoFe_2O_4$	OER	1 M KOH	1T	current density increases by 0.6%-0.8%	4
$Co_{2.75}Fe_{0.25}O_4$/$Co(Fe)O_xH_y$	OER	1 M KOH	0.5 T	current density has been improved by 20%	5
CoNi@C Nanosheets	OER	1 M KOH	360 mT	the overpotential decreased by 14 mV@10 mA cm^{-2}	6
Pt	ORR	0.05 M H_2SO_4	0.56 T	current density was increased by about 50%	7
Fe, Co and Zn microcrystals	ORR	0.5 M H_2SO_4	360 mT	the current of Fe, Co and Zn was increased by 12, 8 and 3%	8
carbon paper with Pt catalyst	ORR	-	0.5 T	diffusion of the O_2 was influenced	9
CoPt nanowires in an alumina membrane	ORR	alkaline medium (pH = 8.4)	20-25 mT	the maximum reaction current was enhanced by up to 200%	10

Fe_3O_4, γ-Fe_2O_3, and Fe-N-C	ORR	0.1 M KOH	0-0.56 T	currents of Fe_3O_4, γ-Fe_2O_3, and Fe-N-C were increased by 21.8, 22.7, and 26.3%	11
Co_3O_4/ECNFs	ORR	20 mM KCl solution	0-1.32 mT	the number of exchanged electrons was increased from 3.48 to 3.92	12
magnetic catalytic nanocages	ORR	0.1 M KOH	350 mT	the half wave-potential is increased by 20 mV	13
Ni-W alloys	HER	1 M KOH	0.1-0.4 T	cathodic peak current density increased by 0.16 A cm^{-1}	14
bowl-like MoS_2	HER	1 M KOH	0.8 T	the overpotential decreased by 10 mV@-10 mA cm^{-2}	15
$NiFe_2O_4$@MOF-74	HER	1 M KOH	2.3 mT	the overpotential decreased by 31 mV@-10 mA cm^{-2}	16
Dendritic fibrous nanosilica Co_3O_4	HER	1 M KOH	300 mT	highest kinetic enhancement of 650%	17

References

1. Y. Li, L. Zhang, J. Peng, W. Zhang and K. Peng, *J. Power Sources*, 2019, **433**, 226704.
2. F. A. Garcés-Pineda, M. Blasco-Ahicart, D. Nieto-Castro, N. López and J. R. Galán-Mascarós, *Nature Energy*, 2019, **4**, 519-525.
3. H.-b. Zheng, Y.-l. Wang, P. Zhang, F. Ma, P.-z. Gao, W.-m. Guo, H. Qin, X.-p. Liu and H.-n. Xiao, *Chem. Eng. J.*, 2021, **426**, 130785.
4. X. Ren, T. Wu, Y. Sun, Y. Li, G. Xian, X. Liu, C. Shen, J. Gracia, H. J. Gao, H. Yang and Z. J. Xu, *Nat. Commun.*, 2021, **12**, 2608.
5. T. Wu, X. Ren, Y. Sun, S. Sun, G. Xian, G. G. Scherer, A. C. Fisher, D. Mandler, J. W. Ager, A. Grimaud, J. Wang, C. Shen, H. Yang, J. Gracia, H. J. Gao and Z. J. Xu, *Nat. Commun.*, 2021, **12**, 3634.
6. H. Li, S. Liu and Y. Liu, *ACS Sustain. Chem. Eng.*, 2021, **9**, 12376-12384.
7. N. I. Wakayama, T. Okada, J.-i. Okano and T. Ozawa, *JPN J. Appl. Phys.*, 2001, **40**, L269.
8. L. M. A. Monzon, K. Rode, M. Venkatesan and J. M. D. Coey, *Chem. Mater.*, 2012, **24**, 3878-3885.
9. H. Matsushima, T. Iida, Y. Fukunaka and A. Bund, *Fuel Cells*, 2008, **8**, 33-36.
10. N. B. Chaure, F. M. F. Rhen, J. Hilton and J. M. D. Coey, *Electrochem. Commun.*, 2007, **9**, 155-158.
11. L. Wang, H. Yang, J. Yang, Y. Yang, R. Wang, S. Li, H. Wang and S. Ji, *Ionics*, 2016, **22**, 2195-2202.
12. Z. Zeng, T. Zhang, Y. Liu, W. Zhang, Z. Yin, Z. Ji and J. Wei, *ChemSusChem*, 2018, **11**, 580-588.
13. J. Yan, Y. Wang, Y. Zhang, S. Xia, J. Yu and B. Ding, *Adv. Mater.*, 2021, **33**, 2007525.
14. L. Elias and A. Chitharanjan Hegde, *Electrocatalysis*, 2017, **8**, 375-382.
15. W. Zhou, M. Chen, M. Guo, A. Hong, T. Yu, X. Luo, C. Yuan, W. Lei and S. Wang, *Nano Lett.*, 2020, **20**, 2923-2930.
16. H.-b. Zheng, H.-h. Chen, Y.-l. Wang, P.-z. Gao, X.-p. Liu and E. V. Rebrov, *ACS Appl. Mate. Inter.*, 2020, **12**, 45987-45996.
17. J. Saha, R. Ball and C. Subramaniam, *ACS Sustain. Chem. Eng.*, 2021, **9**, 7792-7802.